Elastic Scattering of Negative Pions by Protons at 230, 290, 370, and 427 Mev*

LESTER K. GOODWIN,† ROBERT W. KENNEY, AND VICTOR PEREZ-MENDEZ
Lawrence Radiation Laboratory, University of California, Berkeley, California
(Received December 5, 1960)

The elastic differential cross section for the scattering of negative pions by hydrogen was measured at laboratory-system pion kinetic energies of 230, 290, 370, and 427 Mev. The elastically scattered pions were detected by a counter telescope which discriminated against recoil protons and inelastic pions on the basis of range. Differential cross sections were obtained at nine angles for each energy and were fitted by a least-squares program to a series of Legendre polynomials. At the three higher energies, D waves are required to give satisfactory fits to the data. The real parts of the forward-scattering amplitudes calculated from this experiment are in agreement with the predictions of dispersion theory. The results of this experiment, in conjunction with data from other pion-nucleon scattering experiments, support the hypothesis of charge independence at these higher energies.

I. INTRODUCTION

THE scattering of pions by nucleons has hitherto been extensively investigated from very low energies up to 300 Mev. In this energy region, dominated by the well-known $(\frac{3}{2},\frac{3}{2})$ resonance, the experimental information is quite consistent and in good agreement with theory.[1]

Above 300 Mev, the data on pion scattering are less complete than at lower energies. There are a few good measurements with high resolution and good statistics up to 330 Mev.[2] Above this energy, much of the published data are qualitative rather than quantitative.[3]

In the experiment described here, the differential elastic-scattering cross section for negative pions on protons has been measured at 230, 290, 370, and 427 Mev (lab) for the incident pion. Also, the differential cross sections for various combinations of the inelastic processes listed below have been measured.

In addition to the elastic-scattering interaction,

$$\pi^-+p\rightarrow\pi^-+p, \tag{1}$$

other competing interactions for π^- incident on protons are the elastic charge exchange,

$$\pi^-+p\rightarrow\pi^0+n, \tag{2}$$

and the inelastic interactions ($\sim$170-Mev threshold) leading to two-pion final states,

$$\begin{aligned}\pi^0+p&\rightarrow\pi^-+\pi^+ +n,\\ &\rightarrow\pi^-+\pi^0+p,\\ &\rightarrow\pi^0+\pi^0+n.\end{aligned} \tag{3}$$

The inelastic cross sections for three-pion final states with a threshold at 345 Mev are negligibly small at the highest energy measured in this experiment (427 Mev).

From these experiments on elastic scattering, information is obtained concerning the amplitudes of the various angular-momentum states in the pion-nucleon interaction at several energies. The rapid increase of one of these waves is consistent with the tentative interpretation that the second resonance in the pion-proton interaction, occurring at 600 Mev,[4,5] is a $D_{\frac{3}{2}}$ resonance.[6]

Comparisons of these experiments with dispersion theory are made in which the D and higher waves in the data analysis are checked with dispersion predictions. The parameters f^2 (pion-nucleon coupling constant) and the zero-energy scattering lengths were given values which are required for good agreement with lower-energy data.[7]

From the combined data for π^-p elastic scattering, for charge exchange, and for π^+p elastic scattering, all at the same energy, one can (as pointed out by Stanghellini[8]) infer a quantitative limit on the validity of the charge-independence hypothesis at these higher energies.

The most complete interpretation of pion-nucleon experiments is based on an analysis in terms of scattering amplitudes and phase shifts. This approach is desirable at the higher energies also, and may be carried out consistently when the higher energy data become adequate. The main complication introduced at higher energies is that additional phase shifts are required and also that they become complex quantities because of the appearance of inelastic channels. For a satisfactory determination of the phase shifts, the possible differential and total inelastic reactions must

* Work done under the auspices of the U. S. Atomic Energy Commission.
† Present address: Aeronutronic, Ford Road, Newport Beach, California.

[1] H. Bethe and F. de Hoffmann, *Mesons and Fields* (Row Peterson and Company, Evanston, Illinois, 1955), Vol. II.
[2] B. Pontecorvo, in Proc. Ninth Intern. Conf. High Energy Phys., Kiev, U.S.S.R., 1959 (unpublished).
[3] R. R. Crittenden, J. H. Scandrett, W. D. Shephard, W. D. Walker, and J. Ballam, Phys. Rev. Letters **2**, 121 (1959).
[4] T. J. Devlin, B. C. Barish, W. N. Hess, V. Perez-Mendez, and J. Solomon, Phys. Rev. Letters **4**, 242 (1960).
[5] J. C. Brisson, J. Detoef, P. Falk-Vairant, L. van Rossum, G. Valladas, and L. C. L. Yuan, Phys. Rev. Letters **3**, 561 (1959).
[6] W. D. Walker, J. Davis, and W. D. Shephard, Phys. Rev. **118**, 1612 (1960).
[7] H. J. Schnitzer and G. Salzman, Phys. Rev. **112**, 1802 (1958).
[8] A. Stanghellini, Nuovo cimento **10**, 398 (1958).

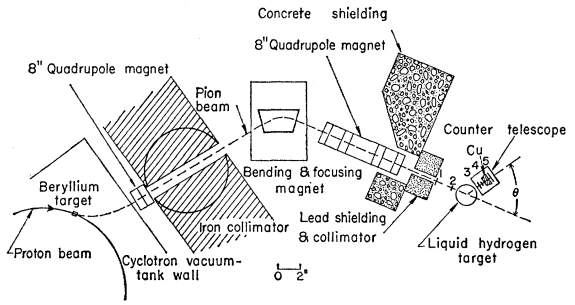

FIG. 1. Diagram of first-run experimental arrangement.

be known to an accuracy comparable to that for the elastic data. A tentative set of phase shifts up to 600 Mev has been proposed by Walker, based on the existing elastic and inelastic data.[6] This set can be significantly improved when missing or uncertain data are determined as accurately as the elastic-scattering data in this and similar experiments.[9]

II. EXPERIMENTAL METHOD

A. Experimental Arrangement

1. *Magnets and Collimators*

A diagram of the experimental arrangement at the Berkeley synchrocyclotron is shown in Fig. 1. The 730-Mev proton beam produced π^- mesons in the beryllium internal target which was 2 in. thick in the direction of the beam. The negative pions were deflected out of the cyclotron by its magnetic field, through a thin aluminum window in the vacuum tank, focused by a quadrupole magnet, and then passed through an iron collimator 8 ft long.

The pion beam was momentum-analyzed and focused by passing through a conventional horizontal magnet system,[10] after which the beam passed through a collimating hole in a 2-ft-thick lead wall. At each energy, the pion flux at the position of the hydrogen target was in excess of 10^4 pions/sec in a 2-in. diameter beam.

2. *Pion Beams*

The energies of the four pion beams are listed in Table I with their energy spreads and contaminations. The average energy, the energy spread, and the fractional muon contamination of each pion beam were determined from range measurements in copper.

The electron contaminations were measured directly at the two lower energies by using a gas Čerenkov counter set to count particles of $\beta > 0.99$.[11] At the two higher energies, upper limits to the number of electrons in the beam were estimated.

TABLE I. Energies and contaminations of π^- beams.

Pion beam energy, lab (Mev)	Use of beam	Muon contamination (%)	Electron contamination (%)
230±6	Data run	15±1	5±1
290±7	Data run	8±1	1±1
370±9	Data run	4±1	1±1
427±10	Data run	4±2	1±1
120±7	Calibration	3±3	···
155±5	Calibration	38±3	···
192±7	Calibration	13±2	···
294±6	Calibration	5±1	···
378±9	Calibration	4±1	···

Horizontal and vertical beam profiles were measured at the position of the liquid hydrogen target with a $\frac{1}{4}$-in. square counter placed in coincidence with the two beam-monitor counters.

3. *Counters*

All the counters, with the exception of the gas Čerenkov counters, were plastic scintillators viewed through Lucite light pipes by RCA 6810A photomultiplier tubes. The sizes of the scintillators shown in Fig. 1 are listed in Table II.

During the data runs, counters 1 and 2 were used as monitors, and counters 3, 4, and 5 were combined into a counter telescope to detect elastically scattered pions. These counters were placed as shown in Fig. 2. The details of the counter-telescope design are discussed below.

4. *Electronics*

A block diagram of the electronics is shown in Fig. 3. The high counting rates, up to 10^6 counts/sec, required high-speed electronic circuits.[12] The correction for

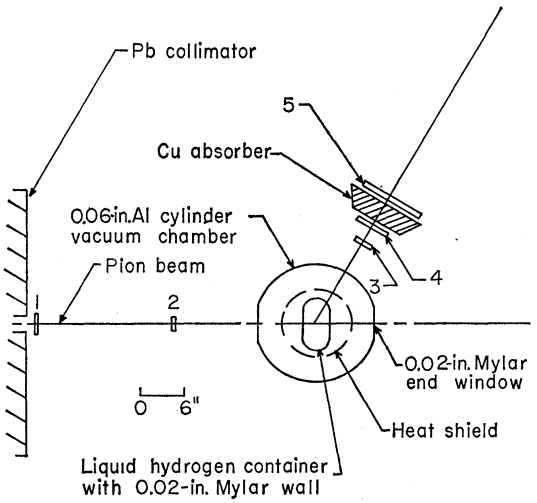

FIG. 2. Diagram showing the details of the hydrogen target and counter arrangement.

[9] J. C. Caris, R. W. Kenney, V. Perez-Mendez, and W. A. Perkins, Phys. Rev. **121**, 893 (1961).
[10] W. G. Cross, Rev. Sci. Instr. **22**, 717 (1951).
[11] J. H. Atkinson and V. Perez-Mendez, Rev. Sci. Instr. **30**, 865 (1959).
[12] D. F. Swift and V. Perez-Mendez, Rev. Sci. Instr. **30**, 865 (1959).

TABLE II. Dimensions of scintillation counters (in.).

Counter	Width	Height	Diameter	Thickness
1	3.00	3.00		0.25
2			2.00	0.25
3	3.00	4.00		0.50
4	6.00	6.00		0.50
5	11.00	12.00		0.50

multiple counts in one fine-structure pulse is discussed under Corrections.

Both fourfold coincidences, 1234, and fivefold coincidences, 12345, were recorded in addition to the monitor doubles, 12. During measurements at forward angles, a $\frac{1}{4}$-in.-thick anticoincidence counter with a 2-in.-diam hole was used to define the incident beam more accurately. It was placed just before the target to reduce direct beam spray into the telescope.

5. *Target*

The liquid hydrogen target consisted of a small container with vertical side walls 5 in. high made of 0.02-in.-thick Mylar (Fig. 2). Copper top and bottom plates (4 in. wide and 8 in. long with 2-in. radius ends) supported the Mylar walls, which were bonded to these plates with a Versamid epoxy mixture. The container was thermally insulated by a vacuum.

A correction for bulging of the Mylar walls in the vacuum, due to the 1-atm pressure inside the target, was included in determining the target thickness.

B. Counter Telescope

1. *Design*

The counter telescope consisted of scintillation counters 3, 4, and 5, as shown in Fig. 2. It pivoted as a unit in the horizontal plane about the center of the hydrogen target. The distance from this pivot axis to the telescope was variable so that the solid angle subtended could be adjusted.

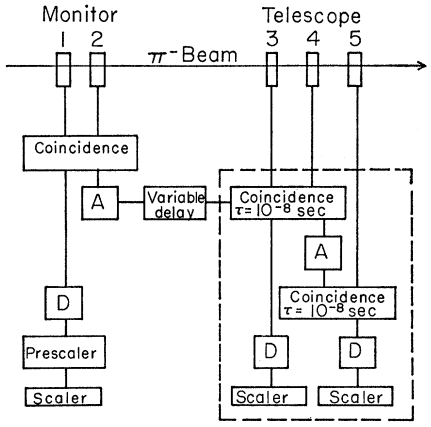

FIG. 3. Block diagram of electronics for monitor and counter telescope. A = amplifier; D = discriminator (see reference 12).

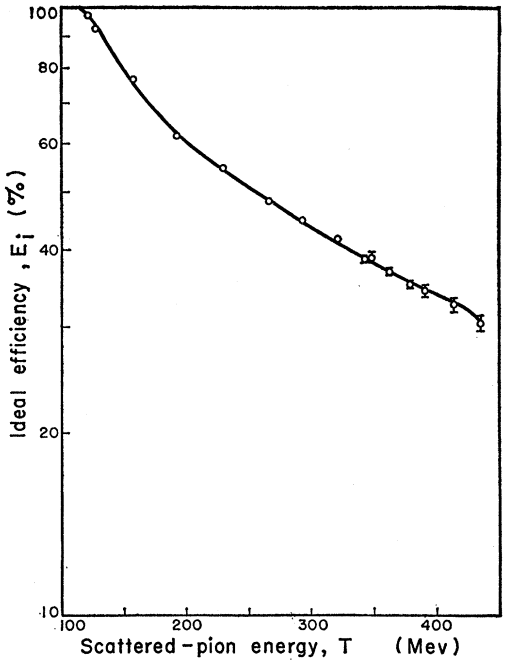

FIG. 4. Counter-telescope efficiency for the ideal amount of Cu absorber as a function of the energy of the elastically scattered pions.

In order to distinguish the elastically scattered pions [interaction (1)] from their recoil protons and the other charged particles produced [interactions (3)], copper absorbers were placed between counters 3 and 5 in the telescope. The elastically scattered pions have greater range than any of the other secondary particles at a given laboratory-system angle; hence the absorber thickness was chosen to allow only the elastically scattered pions to reach counter 5.

Two-body kinematic equations were used to find the maximum energy of pions from interactions (3) by taking as the mass of one of the outgoing particles the sum of a pion mass and a nucleon mass.

The minimum amount of copper absorber needed in the counter telescope was approximately the same for a given kinetic energy of elastically scattered pions independent of the energy of the incident pion beam. It was found that the thickness of copper needed was less than that given by the simple linear equation

$$C_i = (T-100)/2, \tag{4}$$

where C_i (in g/cm²) is the ideal amount of absorber and T is the kinetic energy (lab) (in Mev) of the elastically scattered pions. Consequently, the amount of absorber determined from Eq. (4) was used throughout the experiment.

Counters 4 and 5 were large enough that losses from multiple Coulomb scattering in the absorbers were less than 0.5%.

2. *Calibration*

For the highest-energy scattered pions, the required amount of copper absorber in the telescope transmitted only about $\frac{1}{3}$ of the pions. Consequently, it was of great importance to measure accurately the efficiency of the counter telescope throughout its range of use.

The absolute calibration of the counter telescope was carried out with essentially the same beam setup as shown in Fig. 1 by placing the telescope directly in the main pion beam just after the monitor counters and varying the π^- beam energy from 100 to 430 Mev.

On the assumption that the muons are counted with 100% efficiency, the counter efficiency E is related to the measured fraction transmitted, F, and the fractional beam contamination, K, by

$$E=(F-K)/(1-K). \quad (5)$$

The results of the measurements for establishing the curves used to calibrate the counter efficiency are given in Table I and Fig. 4. The unusually high muon contamination at 155 Mev reflected the physical impossibility of properly adjusting the position of the internal beryllium target at this energy.

C. Experimental Procedure

1. *Accidentals and Background*

The only important accidentals counting rate in this experiment is due to more than one particle passing through the monitor during a single cyclotron rf fine-structure pulse. This rate was measured by appropriate electronic delay procedures and taken into account in the data reduction.

The background counts during the run were measured by cycling with the target empty and full at each different laboratory-system angle. This was done for both regular and accidentals runs.

2. *Counting Rates*

The counting rate for scattered pions was of the order of 10 counts/min. Singles counting rates were regulated with regard for the observed accidentals rates.

D. Related Measurements

1. *Simultaneous Experiments*

While this experiment was being carried out on one side of the hydrogen target, other experiments were performed on the other side.

During the data run at 230 and 290 Mev, the charge-exchange process given in interaction (2) was measured.[9] During the data run at 370 and 427 Mev, the π^+ production processes given in interactions (3) were measured.[13]

[13] W. A. Perkins, J. C. Caris, R. W. Kenney, and V. Perez-Mendez, Phys. Rev. **118**, 1364 (1960).

TABLE III. π^- elastic-scattering differential cross sections.

Beam energy (Mev)	Lab. angle, θ (deg)	$I_A \pm \Delta I_A$ ($\times 10^6$)	$d\sigma/d\Omega_T$ $\pm\Delta d\sigma/d\Omega_T$ (mb/sterad)	$d\sigma/d\Omega^*$ $\pm\Delta d\sigma/d\Omega^*$ (mb/sterad)	C.m. angle, θ^* (deg)
230	15.0	14.75±1.36	4.70±0.43	3.03±0.30	20.1
	22.4	24.90±1.24	4.58±0.23	3.14±0.17	30.0
	38.0	16.01±0.73	2.76±0.13	2.11±0.11	50.0
	54.6	24.00±0.85	1.64±0.06	1.45±0.06	70.0
	72.7	13.18±0.47	0.84±0.03	0.89±0.04	90.0
	92.7	16.18±0.64	0.80±0.03	1.06±0.05	110.0
	114.8	20.98±0.78	0.90±0.03	1.48±0.07	130.0
	139.5	28.02±0.84	1.06±0.03	2.11±0.07	150.0
	159.4	12.29±0.49	1.03±0.04	2.23±0.10	165.0
290	15.0	8.28±1.71	2.99±0.62	1.67±0.33	20.8
	21.8	15.97±1.02	3.35±0.21	1.99±0.12	30.0
	36.9	10.58±0.66	2.15±0.13	1.43±0.08	50.0
	53.2	18.65±0.97	1.49±0.08	1.16±0.06	70.0
	70.9	11.67±0.58	0.80±0.04	0.77±0.04	90.0
	90.8	8.03±0.39	0.48±0.02	0.58±0.02	110.0
	113.2	9.89±0.45	0.50±0.02	0.78±0.03	130.0
	138.3	14.87±0.75	0.65±0.03	1.25±0.05	150.0
	158.8	8.03±0.45	0.77±0.04	1.63±0.08	165.0
370	10.4	2.23±0.56	2.68±0.67	1.14±0.33	15.0
	20.9	10.27±0.53	2.68±0.14	1.38±0.07	30.0
	35.5	20.08±1.13	2.14±0.12	1.26±0.07	50.0
	51.3	16.02±0.74	1.50±0.07	1.06±0.05	70.0
	68.7	9.20±0.45	0.75±0.04	0.67±0.03	90.0
	88.4	5.56±0.26	0.39±0.02	0.45±0.02	110.0
	111.0	6.83±0.30	0.41±0.02	0.63±0.03	130.0
	136.7	7.49±0.41	0.39±0.02	0.74±0.04	150.0
	157.9	3.56±0.27	0.40±0.03	0.87±0.07	165.0
427	10.1	4.24±0.66	4.97±0.78	2.18±0.37	15.0
	20.4	11.16±1.47	3.20±0.42	1.57±0.21	30.0
	34.7	25.81±1.60	2.95±0.18	1.66±0.11	50.1
	50.2	17.31±0.89	1.80±0.09	1.23±0.07	70.2
	67.4	9.64±0.52	0.87±0.05	0.76±0.04	90.2
	87.0	4.74±0.27	0.35±0.02	0.41±0.03	110.2
	109.7	6.02±0.33	0.41±0.02	0.64±0.04	130.2
	135.8	9.58±0.47	0.54±0.03	1.09±0.06	150.1
	157.4	3.86±0.24	0.47±0.03	1.07±0.07	165.1

In order to avoid a possible change in background level, data cycles were completed during periods when no changes were made in these other experiments.

2. *Total Cross Section*

Also in conjunction with this experiment, the total cross section was measured. This was done by using the same pion beam arrangement and magnet setting as in measurements of the differential cross section. The hydrogen target was replaced by a long (4 ft) hydrogen target.[14] This measurement is described elsewhere.[15] The importance of the measurements to this experiment is that the beams for which total cross sections were obtained were identical to those for which the elastic-scattering cross section was measured. These two results are then compared by using the dispersion relation (15), and the comparison is sharpened by being

[14] D. D. Newhart, V. Perez-Mendez, and W. L. Pope, University of California Radiation Laboratory Report UCRL-8857 (unpublished).

[15] J. C. Caris, L. K. Goodwin, R. W. Kenney, V. Perez-Mendez, and W. A. Perkins, Phys. Rev. **122**, 262 (1961).

independent of pion beam characteristics. Independent of the uncertainties in determining these energies, dispersion relations are discussed.

III. RESULTS

A. Differential Cross Section

The average numbers of scattered particles per monitor count, I_A, at each energy and angle are listed in Table III.

The laboratory-system differential cross section, $d\sigma/d\Omega$, is related to the average scattered counts per monitor count, I_A, by

$$d\sigma/d\Omega = I_A/E\Omega K, \quad (7)$$

where E is the efficiency, Ω is the solid angle subtended by the counter telescope, and K, the target constant, is the number of scattering centers per unit area normal to the beam direction. For hydrogen, it is given by

$$K = N_0 \rho_H L, \quad (8)$$

where N_0 is Avogadro's number, ρ_H is the density of the liquid hydrogen in the target, and L is the average thickness of the target parallel to the beam direction.

The target pressure was about 1 atm at all times. The density, $\rho_H = 69.3 \pm 0.8$ g/liter, used in Eq. (8) was actually taken as the difference between the densities of boiling liquid hydrogen[16] and the hydrogen vapor present when the target was empty.

The effective thickness L of the target was determined by averaging the measured target thickness at 25°K with weights determined from the beam-profile measurements. The average thickness L was 4.230 in. The resultant value for the target constant, K, determined from Eq. (8) is $(4.48 \pm 0.05) \times 10^{23}$ cm^{-2}.

B. Corrections

1. *Finite Target Telescope*

The total cross section is determined from Eq. (7) for a point target and telescope.

To correct for finite target and counter sizes, the product of efficiency and solid angle, $E\Omega$, that appears in Eq. (7) was replaced by an appropriate average value, $\langle E\Omega \rangle_{av}$.

The results obtained for the total scattered-pion differential cross sections in the laboratory system, $d\sigma/d\Omega_T$, are listed in Table IV. These values were obtained from Eq. (7) after $E\Omega$ was replaced by $\langle E\Omega \rangle_{av}$.

2. *Beam Contamination and Attenuation*

The muon and electron contamination of the incoming pion beam, the decay of pions into muons between the monitor and target, and the attenuation of both incident and scattered pions by the target material required that a negative correction be applied to the monitor counting rate, where the monitor is to be regarded as counting only those pions that enter into the scattering experiments. This correction does not change the form of the angular distribution, only its normalization.

The fractional beam contaminations were determined from range measurements, and the values obtained are listed in Table I.

3. *Coulomb Scattering*

At the energies and angles (lab) measured in this experiment, interference between nuclear and Coulomb

TABLE IV. Pion-production differential-cross-section data.

Beam energy (Mev)	Lab angle, θ (deg)	$I_A' \pm \Delta I_A'$ ($\times 10^6$)	$d\sigma_4/d\Omega \pm \Delta d\sigma_4/d\Omega$ (mb/sterad)	$f[d(2\sigma_1+\sigma_2)/d\Omega \pm \Delta d(2\sigma_1+\sigma_2)/d\Omega]$ (mb/sterad)	$\sim f$ fraction	$d(2\sigma_1+\sigma_2)/d\Omega \pm \Delta d(2\sigma_1+\sigma_2)/d\Omega$ (mb/sterad)
230	72.7	22.63±1.29	0.93±0.05	0.09±0.06	0.38±0.17	0.24±0.19
	92.7	22.06±1.34	0.93±0.06	0.13±0.07	0.11±0.15	1.18±1.72
	114.8	23.38±1.08	1.00±0.05	0.10±0.06	0	···
	139.5	24.85±1.01	1.05±0.04	0.01±0.05	0	···
	159.4	11.99±0.92	1.18±0.09	0.15±0.10	0	···
290	70.9	23.53±1.86	0.99±0.08	0.19±0.09	0.79±0.08	0.24±0.12
	90.8	15.95±1.09	0.66±0.05	0.18±0.06	0.69±0.12	0.26±0.10
	113.2	13.32±0.84	0.56±0.04	0.06±0.05	0.52±0.15	0.12±0.11
	138.3	18.75±1.21	0.80±0.05	0.15±0.06	0.33±0.18	0.45±0.31
	158.8	8.48±1.35	0.84±0.14	0.07±0.15	0.21±0.17	0.33±0.76
370	88.4	18.77±0.70	0.77±0.03	0.38±0.04	0.87±0.05	0.44±0.06
	111.0	14.02±0.66	0.60±0.03	0.19±0.04	0.80±0.08	0.24±0.06
	136.7	12.52±0.73	0.53±0.03	0.14±0.04	0.72±0.10	0.19±0.06
	157.9	6.78±0.97	0.67±0.10	0.27±0.11	0.63±0.13	0.43±0.20
427	87.0	22.11±1.02	0.89±0.04	0.54±0.05	0.92±0.03	0.59±0.06
	109.7	18.87±1.07	0.80±0.05	0.39±0.06	0.88±0.05	0.44±0.07
	135.8	19.01±1.06	0.81±0.05	0.27±0.06	0.81±0.07	0.33±0.08
	157.4	6.67±0.92	0.66±0.09	0.19±0.10	0.77±0.09	0.25±0.14

[16] D. B. Chelton and D. B. Mann, University of California Radiation Laboratory Report UCRL-3421 (unpublished).

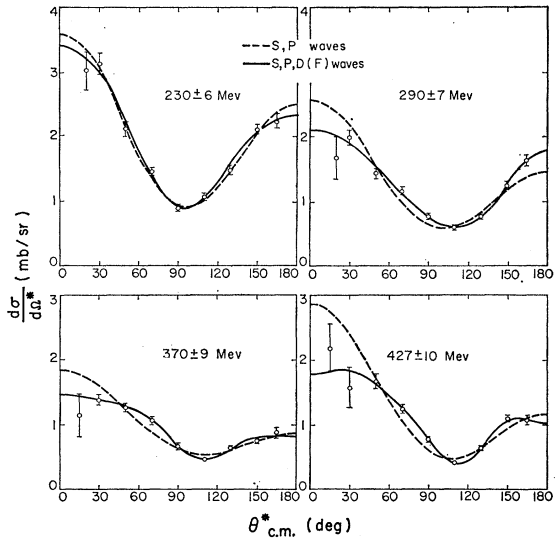

FIG. 5. Differential cross sections of elastically scattered pions for various incident beam energies. Dashed curve is least-squares fit with S and P waves only. Solid curve is best fit.

scattering is negligible,[17,18] and the nuclear contribution can be determined by subtracting the Coulomb cross sections[19] from the measured cross sections.

4. *Charge-Exchange Correction*

The counter telescope is 1% efficient in detecting the reaction $\pi^-+p\rightarrow n+\pi^0\rightarrow n+2\gamma$. The data are corrected for this background by subtracting 1% of the charge-exchange cross section at the same energy.

The final barycentric differential cross section, $d\sigma/d\Omega^*$, and the corresponding center-of-mass angle of scattering, θ^*, are listed in Table III.

C. Errors

1. *Counting Statistics*

The statistical (standard-deviation) errors in the counting data were set equal to the square root of the corresponding number of counts. These errors were propagated to give values of the standard-deviation error ΔI_A, on the average quantities I_A, which are listed in Table IV.

2. *Other Sources of Errors*

The errors in the measured efficiency E, obtained from Eq. (5), depend largely upon the uncertainty ΔK in the beam contamination, since the statistical error in F, the fraction transmitted, is negligible. The error ΔE in the efficiency E is thus given by

$$\Delta E=[(1-F)/(1-K)^2]\Delta K. \qquad (10)$$

This formula has been written down explicitly to show the important fact that the uncertainty in the efficiency is smaller than the uncertainty in the beam-contamination fraction by a factor of about $(1-F)$ for the small values of K observed. Thus the error in the measured efficiency is $\frac{1}{10}$ the beam contamination for efficiencies greater than 90%, for example. As a result, even the uncertainty in the electron contamination of the calibration beam, which was estimated and included as a random-error addition to ΔK, did not give efficiency errors in excess of 4% at any point. At most points, they were less than 2%.

The uncertainty given in the target constant K of Eq. (7) arose primarily from the uncertainty in the temperature of the hydrogen gas in the target when it was not full of liquid hydrogen.

The error in the solid-angle determination was negligible. Small errors arising from the Coulomb and charge-exchange corrections were included.

Both the muon and electron contaminations were evaluated for the pion beams used in the data runs (Table I). The errors in these contaminations appear directly as errors in the correction factor multiplying the total angular distribution. Since they did not exceed 2%, however, they were included for convenience as additional random errors in the individual values of differential cross sections because their contribution is small.

The combined results of all of these errors are listed as standard-deviation errors, $\Delta d\sigma/d\Omega^*$, on the final differential cross-section points, $d\sigma/d\Omega^*$, in Table III. A plot of these differential cross sections is shown in Fig. 5.

D. Pion-Production Cross Sections

Though this experiment was not primarily intended to measure cross sections for any of the pion-production processes given in interactions (3), some information about them is available from quadruple-coincidence (1234) data. No copper absorber was placed between counters 3 and 4 at angles greater than 60 deg (lab). Thus, all charged particles from reactions (1) and (3) were counted that had an energy above some threshold energy (approximately 25 Mev) necessary to penetrate the target walls as well as counters 3 and 4. No recoil protons can appear at angles greater than 90 deg (lab). Consequently, back of 90 deg (lab) and even at the smaller lab angles, where recoil protons have energies below the detection threshold, only charged pions from interactions (1) and (3) are counted by counters 3 and 4.

Thus if at a lab angle θ the elastic differential cross section is $d\sigma/d\Omega_T$, and the differential cross section for the first of interactions (3) is $d\sigma_1/d\Omega$ and for the second is $d\sigma_2/d\Omega$, then the measured quantity obtained from the quadruple-coincidence data, $d\sigma_4/d\Omega$, is given, to a first approximation, by

$$d\sigma_4/d\Omega=d\sigma/d\Omega_T+f(2d\sigma_1/d\Omega+d\sigma_2/d\Omega), \qquad (11)$$

[17] G. F. Chew and H. P. Noyes, Phys. Rev. **109**, 566 (1958).
[18] H. P. Noyes, Phys. Rev. **111**, 944 (1958).
[19] B. Rossi, *High Energy Particles* (Prentice Hall, Inc., Englewood Cliffs, New Jersey, 1952), p. 64.

where f is the fraction of pions from interactions (3) that have an energy above the threshold energy for detection.

Since $d\sigma/d\Omega_T$ has been determined in this experiment (Table III), and data concerning $d\sigma_1/d\Omega$ were obtained elsewhere,[13] information about $d\sigma_2/d\Omega$ was estimated.

Consequently, the quadruples data 1234 were analyzed in the same way as the quintuples data to get values for $I_A' \pm \Delta I_A'$ for the quadruples data. These values are listed in Table IV. These quantities in turn were used to find $d\sigma_4/d\Omega \pm \Delta d\sigma_4/d\Omega$ from Eq. (7) in the same way as $d\sigma/d\Omega_T \pm \Delta d\sigma/d\Omega_T$ was obtained for the quadruples data, except that the efficiency was assumed to be 100% since there was no absorber between counters 3 and 4. The results are listed in Table IV for meaningful angles. From the results listed in Table III, values for the quantity $f(2d\sigma_1/d\Omega + d\sigma_2/d\Omega)$ were then calculated by means of Eq. (11). These values are listed in Table IV.

It is necessary to evaluate the fraction $f(\theta)$ appearing in Eq. (11). Because of the large statistical errors in all these data, for simplicity the laboratory-system energy spectrum at all angles was assumed to have the approximate form $\sin(2\pi T/T_{\max})$, where T, the kinetic energy of the pion at that angle, has a maximum value $T_{\max}$. Thus, the fraction detected, $f(\theta)$, is given by

$$f(\theta) = [\cos(2\pi T_{\text{th}}/T_{\max}) + 1]/2, \qquad (12)$$

where T_{th}, the energy threshold for detection, is taken as 25 ± 5 Mev. The values of f obtained from Eq. (12) are listed in Table IV.

By using Eqs. (11) and (12) values for the quantity $d(2\sigma_1 + \sigma_2)/d\Omega$ were obtained, and are listed in Table IV. A plot of these points is shown in Fig. 6.

IV. CONCLUSIONS

A. Partial Waves

To determine which angular-momentum states are present in the elastic-scattering interaction at these energies, a Legendre polynomial series of the form

$$\frac{d\sigma}{d\Omega^*}(\theta^*) = \sum_{l=0}^{n} A_l P_l(\cos\theta^*), \qquad (13)$$

was fitted by the method of least squares to the measured differential cross sections, $d\sigma/d\Omega^*$ (Table III) at each beam energy. This form is equivalent to the expansion in Eq. (16) and is simpler. The magnitude of n necessary for an adequate fit to the data points at each energy was determined on the basis of a χ^2 test and supporting Fisher test. The values of coefficients A_l obtained for various values of n at each energy are listed in Table V. Also listed in this table are the degrees of freedom k; the values of χ^2 obtained; the probability p that χ^2 would exceed the value found in a random sample, and the Fisher probability F that A_n should be zero.

The first adequate and best fits determined on the basis of these statistical criteria are indicated by superscripts a and b in Table V. For the best fits, the error matrices, C_{ij}, are given in Table VI. The theoretical curves obtained from Eq. (13) for S and P waves alone ($n=2$) and for the best fits are shown in Fig. 5.

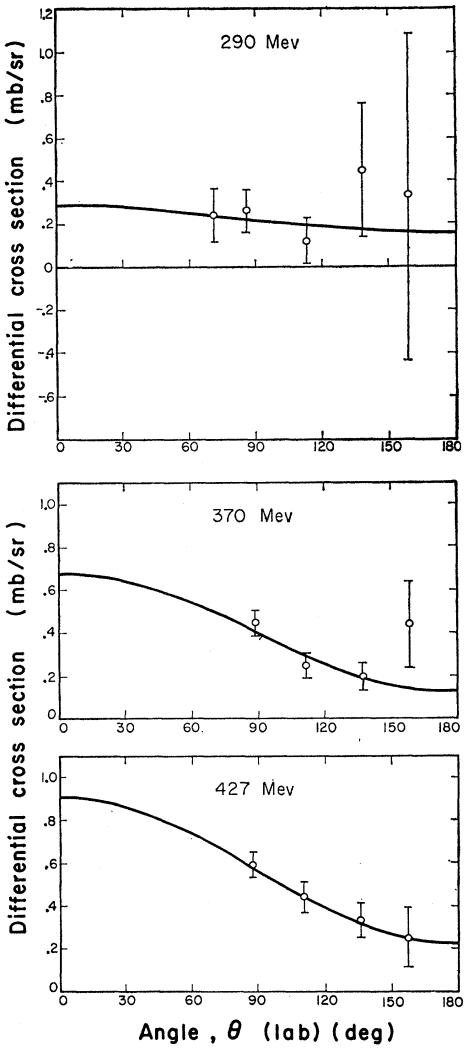

FIG. 6. Combined inelastic differential cross sections, $d(2\sigma_1 + \sigma_2)/d\Omega$, for various incident beam energies. Solid curves represent least-squares fits to a Legendre polynomial series.

At 290 Mev and above, it can be seen that the probability that the data are consistent with fits based on S and P waves alone is less than 1%. In fact, the most probable values of n obtained include an F-wave interference term ($n=5$) at 370 Mev and an F-wave term ($n=6$) at 427 Mev. Thus the conclusion can be drawn that at 230 Mev only S and P waves are needed, but at the higher energies D waves are present and above 290 Mev F waves may be present, especially at 427 Mev.

The total elastic cross section, σ_E, obtained by integrating the best-fit curve for the differential cross

TABLE V. Results of least-squares Legendre-polynomial fits to elastic π^-p data.

Beam energy (Mev)	Order of fit n	Fitted coefficients A_0	A_1	A_2	A_3 (mb/sterad)	A_4	A_5	A_6	χ^2	k	p (%)	F (%)
230±6	2[a]	1.65±0.03	0.55±0.06	1.40±0.06					9.47	6	22	<1
	4[b]	1.66±0.03	0.53±0.06	1.38±0.07	−0.01±0.08	−0.15±0.09			5.82	4	29	20
290±7	3[a]	1.09±0.02	0.44±0.05	0.70±0.05	−0.34±0.05				6.72	5	29	<1
	4[b]	1.10±0.02	0.45±0.05	0.75±0.06	−0.28±0.07	0.11±0.06			3.86	4	41	15
370±9	4[a]	0.86±0.02	0.45±0.03	0.32±0.04	−0.32±0.05	−0.16±0.05			7.43	4	12	7
	5[b]	0.86±0.02	0.45±0.03	0.33±0.04	−0.26±0.06	−0.10±0.07	0.11±0.06		3.97	3	29	15
427±10	5[a]	1.04±0.03	0.63±0.07	0.58±0.08	−0.36±0.10	0.01±0.10	0.24±0.08		4.58	3	21	8
	6[b]	1.04±0.03	0.62±0.07	0.57±0.09	−0.39±0.10	−0.06±0.11	0.15±0.11	−0.12±0.10	3.05	2	23	35

[a] First adequate fit.
[b] Best fit.

section is given by

$$\sigma_E = 4\pi A_0, \tag{14}$$

where A_0 is the coefficient of the constant term ($P_0(\cos\theta^*)=1$). The total elastic cross sections obtained by Eq. (14) are listed in Table VII. The differential cross sections at zero degrees, $d\sigma/d\Omega^*(0)$, obtained from Eq. (13) by setting $\theta=0$ and propagating errors using the error matrix, are also listed in Table VII.

B. Dispersion Relations

Dispersion theory relates the differential forward-scattering cross section, $d\sigma/d\Omega^*(0)$, to the total cross section, σ_T, at the same energy by the dispersion relation

$$d\sigma/d\Omega^*(0) = D^2 + [(k/4\pi)\sigma_T]^2, \tag{15}$$

where k is the momentum of the incident pion in the barycentric system and D is the real part of the forward-scattering amplitude for which values are predicted by the dispersion theory.[20] The units employed in Eq. (15) are those with $\hbar=c=M_\pi=1$.

Equation (15) may be used to determine values for the real part of the forward-scattering amplitude, D, from measured values of the forward differential cross section and the total cross section. Measured values of the forward differential cross section were taken from Table VII, and the total-cross-section values measured

TABLE VI. Best-fit error matrices, C_{ij}.

Beam energy (Mev)	i	j 0	1	2	3	4	5	6
230	0	0.00086	0.00099	0.00107	0.00062	−0.00012		
	1		0.00388	0.00286	0.00190	0.00127		
	2			0.00556	0.00356	0.00250		
	3				0.00702	0.00339		
	4					0.00763		
290	0	0.00049	0.00072	0.00057	0.00009	0.00011		
	1		0.00218	0.00175	0.00135	0.00052		
	2			0.00386	0.00296	0.00187		
	3				0.00434	0.00237		
	4					0.00399		
370	0	0.00029	0.00033	0.00019	−0.00004	−0.00001	0.00012	
	1		0.00108	0.00060	0.00047	0.00020	0.00023	
	2			0.00186	0.00155	0.00123	0.00052	
	3				0.00358	0.00261	0.00195	
	4					0.00423	0.00219	
	5						0.00358	
427	0	0.00093	0.00161	0.00148	0.00077	0.00035	0.00029	0.00008
	1		0.00456	0.00421	0.00313	0.00175	0.00070	0.00051
	2			0.00723	0.00629	0.00430	0.00199	0.00050
	3				0.00981	0.00802	0.00520	0.00213
	4					0.01206	0.00882	0.00537
	5						0.01208	0.00741
	6							0.01001

[20] James W. Cronin, Phys. Rev. **118**, 824 (1960).

at the same energies[15] were used and are also listed in Table VII. The calculated values of D_- are plotted in Fig. 7. Recent theoretical values[20] of D_- obtained by using the latest values of the $\pi-p$ total cross sections at higher energies[4,5] in the dispersion integrals are also shown in Fig. 7 for comparison. Within statistics, no disagreement with these values, and to this extent no disagreement with dispersion theory, is found.

C. Charge Independence

A test for charge independence, given by Stanghellini,[8] consists of relating various scattering amplitudes for $\pi-p$ interactions. In his notation, the right-hand side of his equation, a_R, and the left-hand side,

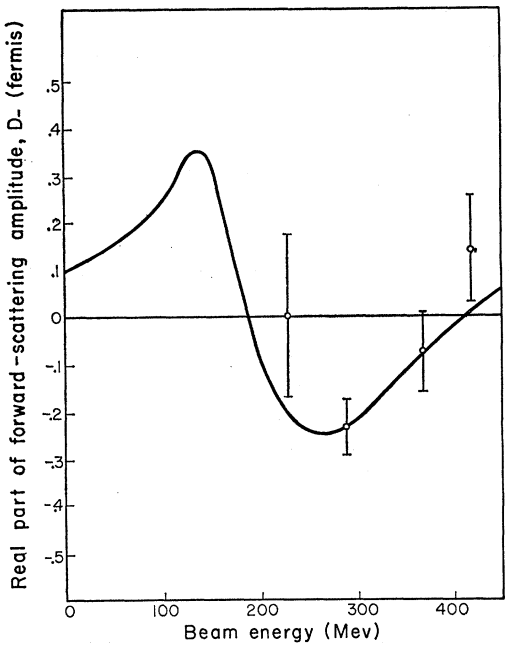

FIG. 7. The real part of the forward-scattering amplitude. Solid curve represents the theoretical values.[20]

a_L, are evaluated from experimental results and compared. By use of the values for π^+-p scattering cross sections at 360 Mev[21] in conjunction with π^--p charge-exchange data at 371 Mev,[9] the following values were calculated for a_R and a_L from the π^--p elastic data obtained in this experiment: $a_R=0.27\pm0.09$ and $a_L=0.39\pm0.02$. His comparison quantity Δ then has the value $\Delta=24\%$. This can be interpreted to mean that the equation is valid within 24%, which is more accurate than the 33% error in its right-hand side, a_R. Thus no disagreement with charge independence is found at 370 Mev. Data available at 427 Mev are not sufficient for this test.

[21] N. S. Mitin and E. L. Grigor'ev, Soviet Physics—JETP **5**, 378 (1957).

TABLE VII. Total elastic and forward differential cross section from best least-squares fits and total cross sections.

Beam energy (Mev)	$\sigma_E\pm\Delta\sigma_E$[a] (mb)	$\frac{d\sigma}{d\Omega^*}(0)\pm\Delta\frac{d\sigma}{d\Omega^*}(0)$[a] (mb/sr)	$\sigma_T\pm\Delta\sigma_T$[b] (mb)
230	20.8±0.4	3.40±0.25	58±9
290	13.8±0.3	2.12±0.20	33±2
370	10.9±0.2	1.41±0.20	27±2
427	13.0±0.4	1.81±0.43	27±2

[a] This experiment.
[b] Caris *et al.*[15]

D. Phase Shifts

If we assume charge independence to be valid, the general formula for pion-nucleon scattering can be written[22]

$$d\sigma/d\Omega^*=\lambda\!\!\!^{-2}\{|\sum_{\tau=\frac{1}{2}}^{\frac{3}{2}}C_\tau\sum_{l=0}^{L}[(l+1)a_{j=l+\frac{1}{2}}{}^{l,\tau}+la_{j=l-\frac{1}{2}}{}^{l,\tau}]P_l{}^0(\cos\theta^*)|^2+|\sum_{\tau=\frac{1}{2}}^{\frac{3}{2}}C_\tau\sum_{l=1}^{L}[(a_{j=l+\frac{1}{2}}{}^{l,\tau}-a_{j=l-\frac{1}{2}}{}^{l,\tau}]P_l{}^1(\cos\theta^*)|^2\}, \quad (16)$$

where the amplitude a is given in terms of its phase shift δ by

$$a=(e^{2i\delta}-1)/2i=e^{i\delta}\sin\delta, \quad (17)$$

and where $\lambda\!\!\!^{-}$ is the wavelength of the pion ($\lambda\!\!\!^{-}=\hbar/k$), τ is the total isotopic spin, C_τ is an appropriate product of Clebsch-Gordan coefficients for the particular interaction considered, L is the maximum-order angular-momentum state that enters, and the P's are Legendre polynomials. The values of C_τ for various pion-nucleon interactions are given in Table VIII.

In Eq. (16) there are present $4L+2$ phase shifts. Elastic π^--p data alone can be fitted with only $2L+1$ parameters. Consequently, π^--p charge exchange or π^+-p scattering data are also needed for determination of all the phase shifts. At the higher energies, at which pion inelastic processes enter, these phase shifts also have nonzero imaginary parts. Pion-production data must then be included to evaluate these imaginary components. More than one acceptable set of solutions may be found as a rule, and polarization data are then needed to resolve these ambiguities. Tracking is necessary, i.e., phase shifts must vary continuously

TABLE VIII. Clebsch-Gordan product coefficients, C_τ.

Interaction	$C_{\frac{3}{2}}$	$C_{\frac{1}{2}}$
$\pi^-+p\to\pi^-+p$	$\frac{2}{3}$	$\frac{1}{3}$
$\pi^-+p\to\pi^0+n$	$-\sqrt{2}/3$	$\sqrt{2}/3$
$\pi^++p\to\pi^++p$	0	1

[22] E. M. Henley, M. A. Ruderman, and J. Steinberger, Ann. Rev. Nuclear Sci. **3**, 12 (1953).

from established values as energy increases. Before one can use available data for the different interactions measured at slightly different energies, they must be properly extrapolated to corresponding energies. The paucity of accurate data, especially on inelastic reactions,[13] currently available above 300 Mev leads to large uncertainties in the derived phase shifts.

However, this problem has been undertaken by Walker *et al.*[6] in the energy region from 300 to 600 Mev. The 370- to 427-Mev results of this experiment already reported[23] have been used in conjunction with data taken by Crittenden *et al.*[3] and by others to obtain one set of phase shifts tracked from lower-energy solutions. Of particular interest here is the approximate equivalence within statistics of the two D-wave phase shifts, δ_{15} and δ_{35}, obtained through 430 Mev. This equivalence supports the possibility that an accidental cancellation may be the reason why no evidence for D waves was found in the charge-exchange results through 371 Mev[9] by partial-wave analysis, although definite evidence has been found here for their presence in the elastic scattering at 290 Mev and above. This may be seen as follows.

If the D-wave phase shifts, δ, are assumed to be small, then Eq. (17) may be approximated for D waves by

$$a_D \approx \delta. \tag{18}$$

If all phase shifts higher than D waves are then assumed to be zero, the A_4 coefficient in Eq. (13) is given from Eq. (16) for charge exchange and using Eq. (18) by

$$A_4 = (4/7)\lambda^2(\delta_{15}-\delta_{35})[4(\delta_{13}-\delta_{35})+(\delta_{15}-\delta_{35})]. \tag{19}$$

Equation (19) shows that when δ_{15} equals δ_{35}, the coefficient A_4 is zero. Consequently the absence of a pure D-wave term in the charge-exchange partial wave results does not imply the absence of D waves even though its presence does indicate that D waves exist. Thus there is probably no basic conflict between the elastic and charge-exchange results through 371 Mev.

Theoretical values for the D-wave phase shifts have been predicted by Chew *et al.* on the basis of dispersion theory.[24] These values do not agree with those found by Walker *et al.*[6] However, one could not expect good agreement of these theoretical phase shifts because the effects of possible pion-pion interactions were neglected. Recent results indicate the importance of such interactions at these energies,[13] and the disagreement found can be attributed to them.

[23] L. K. Goodwin, R. W. Kenney, and V. Perez-Mendez, Phys. Rev. Letters **3**, 522 (1959).
[24] G. F. Chew, M. L. Goldberger, F. E. Low, and Y. Nambu, Phys. Rev. **106**, 1337 (1957).

TABLE IX. Pion-production total cross section.

Beam energy (Mev)	Total cross sections (mb) $2\sigma_1+\sigma_2$	σ_1	$\sigma_1+\sigma_2$	σ_2
290	2.8±0.8	0.4 ±0.2	2.4±0.8	2.0±0.9
370	5.0±0.7	1.93±0.37	3.1±0.8	1.2±1.0
427	7.1±0.7	3.36±0.74	3.7±1.0	0.4±1.6

E. Pion-Production Processes

Measured values of the combined pion-production differential cross sections $d(2\sigma_1+\sigma_2)/d\Omega$, are listed in Table IV and shown in Fig. 6. Because of the complications introduced by the three-body pion-production kinematics, no attempt was made here to separate the two differential cross sections or convert them to the barycentric system by using previously measured values of $d\sigma_1/d\Omega^*$. Rather, a Legendre polynomial series of the form

$$d(2\sigma_1+\sigma_2)/d\Omega = A_0'P_0(\cos\theta)+A_1'P_1(\cos\theta) \tag{20}$$

was fitted to the combined laboratory-system differential cross section [see Eq. (3)], where the cross sections σ_1, σ_2, σ_3 apply to the first, second, and third reactions, respectively, and an excellent fit resulted at all three energies as determined by a χ^2 test. The total cross section, $2\sigma_1+\sigma_2$, was then obtained from Eq. (14), and the results are listed in Table IX.

In Table IX are also given the values of σ_1 previously reported.[13] By subtracting these values from $2\sigma_1+\sigma_2$, the charged-inelastic-pion cross section, $\sigma_1+\sigma_2$, was obtained, and the results are listed in Table IX. These results are in statistical agreement with other published values.[3]

By again subtracting σ_1 from $\sigma_1+\sigma_2$, values for σ_2 were obtained, and are listed in Table IX. The errors on σ_2 are so large that little can be learned quantitatively. However, qualitatively it appears that σ_2 may be decreasing with energy, and at the higher energies it is significantly smaller than σ_1.

ACKNOWLEDGMENTS

The suggestions and encouragement of Professor A. C. Helmholz throughout the course of this work are gratefully acknowledged. Thanks are due Dr. Walton Perkins III, and Dr. John Caris for their generous help throughout the experimental program. We should also like to thank the many other members of our group who contributed their time during the cyclotron runs.

Finally, we wish to thank Mr. James Vale and the cyclotron crew for their assistance and cooperation during the course of the experimental work.